11th World Congress on Computational Mechanics (WCCM XI)
5th European Conference on Computational Mechanics (ECCM V)
6th European Conference on Computational Fluid Dynamics (ECFD VI)
E. Oñate, J. Oliver and A. Huerta (Eds)

MICRO-MECHANICAL NUMERICAL ANALYSIS OF DUCTILE DAMAGE UNDER DYNAMIC LOADING CONDITIONS

STEFFEN GERKE*, KEVIN KUHNT* AND MICHAEL BRÜNIG*

* Institut für Mechanik und Statik
Universität der Bundeswehr München
Werner-Heisenberg-Weg 39, 85579 Neubiberg, Germany
e-mail: steffen.gerke@unibw.de - Web page: www.unibw.de/baumechanik

Key words: Ductile materials, Damage and fracture, Dynamic loading, Stress triaxiality dependence, Micro-mechanical simulations

Abstract. The paper deals with the damage and fracture behavior of ductile metals under dynamic loading conditions. A phenomenological continuum damage and fracture model is presented which takes into account the rate- and temperature-dependence of the material. This model provides reasonable results of numerical simulations of experiments with high strain rates while the identification of the corresponding material parameters results difficult from the available experimental data. This lack of information can be resolved by micro-mechanical numerical simulations of void containing unit-cells. Thus results of dynamic micro-mechanical simulations are presented which can be used to study the damage effects on the micro-scale and to validate the rate-dependent continuum damage model.

1 INTRODUCTION

The description of the material behavior under general loading conditions becomes increasingly evident with the need to activate its inelastic resources. Thus a detailed knowledge of this inelastic behavior, including the deterioration of the material on the micro-scale, is crucial. In addition it can be observed that these damage and fracture processes frequently occur under dynamic loading conditions which appear for example at high speed machining and at crash or impact processes. For instance Fig. 1 illustrates the microstructure of a ductile metal plate which was impacted in thickness direction [1]. Here it can be noticed that with increasing impact velocity the amount of damage also increases and finally leads to the formation of micro- and macro-cracks.

The simulation of the deformation and failure behavior of complete structures or structural components is usually realized with the finite element method. In this context a

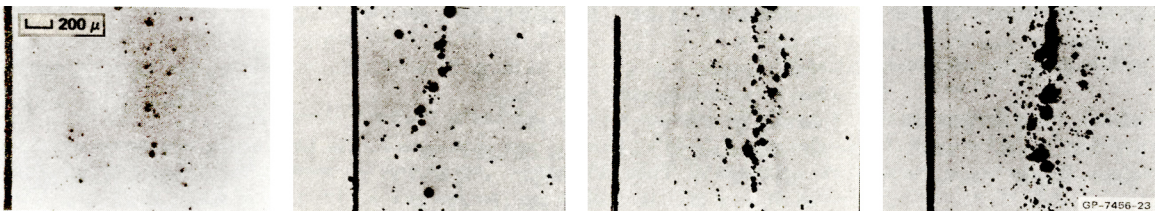

Figure 1: Ductile damage under dynamic loading; Micro structure after impact, impact velocities, left to right: 433 fps, 468 fps, 506 fps and 688 fps; cut-outs from Barbee et al. [1]

phenomenological model is applied, i.e. the behavior of the damaged material is reflected by a continuous material while the ongoing damage is described by corresponding damage rules. The continuum approach is based on experimental observation and also takes into account mechanisms acting on the micro-level.

The micro-mechanisms which lead to the final failure of the material primarily depend on the stress state and thus big effort is made to study these mechanisms experimentally [2, 3]. However, it is not an easy task to develop experiments and corresponding specimens which can be tested at various stress states under well controlled conditions even under static loading conditions. Under dynamic loading conditions the variety of experiments and the available data from these experiments is even more limited. Here frequently Split-Hopkinson-Bar experiments are used with uniaxially loaded specimens either in compression or in tension while further loading conditions are difficult to apply.

To overcome these experimental deficits, frequently micro-mechanical simulations with void containing cells are used to study the damage behavior under general loading conditions [4, 5]. These micro-mechanical simulations under static loading conditions have been successfully used to gain additional information with respect the ongoing damage processes [6] while under dynamic loading conditions only two-dimensional studies have been presented [7].

In the present paper three-dimensional simulations of pore containing micro-cells under dynamic loading conditions are discussed. These unit cells are uniaxially loaded by a tension pulse whereas the influence of several different boundary conditions applied to the surfaces perpendicular to the loading direction are studied. Besides a homogeneous pore distribution several different heterogeneous distributions are simulated resulting in the identification of different damage mechanisms and thus these micro-mechanical studies can be used to validate the continuum damage model under dynamic loading conditions.

2 CONTINUUM DAMAGE MODEL

The continuum model is used to predict the irreversible material behavior while its rate- and temperature-dependence is also taken into account [8, 9]. The phenomenological approach is based on the consideration of damaged as well as fictitious undamaged configurations. The kinematics lead to the additive decomposition of the strain rate tensor into elastic, plastic and damage parts. The effective undamaged configurations are used

to model the elastic-plastic behavior of the undamaged matrix material. Plastic yielding is governed by the yield criterion

$$f^{\mathrm{pl}} = a\bar{I}_1 + \sqrt{\bar{J}_2} - c\left(\gamma, \dot{\gamma}, \theta\right) = 0 \tag{1}$$

which is motivated by experiments realized by Spitzig et al. [10] who studied the plastic behavior of ductile metals under superimposed hydrostatic pressure. In Eq. (1) a is the hydrostatic stress coefficient which depends on the stress state while the ratio a/c is constant [10], $\bar{I}_1 = \mathrm{tr}\bar{\mathbf{T}}$ is the first invariant of the effective stress tensor $\bar{\mathbf{T}}$ and $\bar{J}_2 = \frac{1}{2}\mathrm{dev}\bar{\mathbf{T}} \cdot \mathrm{dev}\bar{\mathbf{T}}$ the second invariant of its deviator. Furthermore $c\left(\gamma, \dot{\gamma}, \theta\right)$ is the equivalent stress measure depending on the equivalent plastic strain γ, the equivalent plastic strain rate $\dot{\gamma}$ and the temperature θ. The rate- and temperature-dependent plastic behavior is described by

$$c\left(\gamma, \dot{\gamma}, \theta\right) = \tilde{c}\left(\gamma\right) f_1\left(\dot{\gamma}\right) f_2\left(\theta\right) \tag{2}$$

which is a multiplicative decomposition into a quasi-static, a temperature-dependent and a rate- dependent part similar to the frequently used Johnson–Cook [11] model. The quasi-static hardening behavior is characterized by the power law

$$\tilde{c}\left(\gamma\right) = \tilde{c}_o \left(\frac{H_o \gamma}{n\tilde{c}_o} + 1\right)^n \tag{3}$$

where $\tilde{c}_o$ represents the initial yield stress, H_o the hardening parameter and n the hardening exponent. The fact that the material reacts stiffer with increasing strain rates is characterized by the strain-rate-hardening function

$$f_1\left(\dot{\gamma}\right) = 1 + d\left(\frac{\dot{\gamma} - \dot{\gamma}_o}{\dot{\gamma}_o}\right)^m \tag{4}$$

valid for $\dot{\gamma} > \dot{\gamma}_o$ where d and m are further material parameters and $\dot{\gamma}_o$ is the strain rate of the quasi-static reference test. The circumstances that with increasing temperature the material reacts softer is characterized by the thermal softening function

$$f_2\left(\theta\right) = 1 - b\ \mathrm{sgn}\left(\frac{\theta - \theta_o}{\theta_m - \theta_o}\right)\left[\mathrm{abs}\left(\frac{\theta - \theta_o}{\theta_m - \theta_o}\right)\right]^q \tag{5}$$

where b and q are further material parameters, θ_o represents the reference temperature and θ_m is the melting temperatur [12]. In addition, the isochoric effective plastic strain rate

$$\dot{\bar{\mathbf{H}}}^{\mathrm{pl}} = \dot{\gamma}\frac{1}{\sqrt{2\bar{J}_2}}\mathrm{dev}\bar{\mathbf{T}} \tag{6}$$

is defined.

Furthermore, corresponding anisotropically damaged configurations are considered characterizing the inelastic deformation behavior of the damaged aggregate. Different damage

mechanisms have been observed depending on the stress state: damage is characterized by shear modes for negative stress triaxialities, by void growth dominated modes for large positive triaxialities, by mixed modes for lower positive stress triaxialities and below a certain cut-off-value no further damage occurs, Fig. 2, [2, 13]. Here the stress triaxiality is defined as $\eta = I_1/\left(3\sqrt{3J_2}\right)$ while $I_1 = \mathrm{tr}\mathbf{T}$ is the first invariant of the Kirchhoff stress tensor $\mathbf{T}$ and $J_2 = \frac{1}{2}\mathrm{dev}\mathbf{T} \cdot \mathrm{dev}\mathbf{T}$ the second invariant of its deviator. Thus, the onset

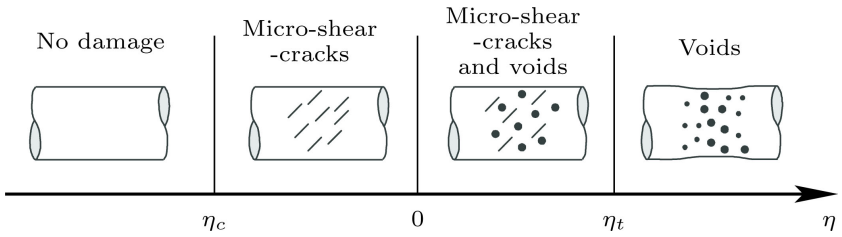

Figure 2: Different damage mechanisms depending on stress triaxiality η

of damage is assumed to be governed by the rate- and temperature-dependent damage criterion

$$f^{\mathrm{da}} = \tilde{\alpha} I_1 + \tilde{\beta}\sqrt{J_2} - \tilde{\sigma}\left(\mu, \dot{\mu}, \theta\right) = 0 \tag{7}$$

where $\tilde{\sigma}\left(\mu, \dot{\mu}, \theta\right)$ is the equivalent damage stress measure, depending on the equivalent damage strain μ, the equivalent damage strain rate $\dot{\mu}$ and the absolute temperature θ. The above mentioned stress triaxiality dependence is reflected by the choice of the parameters

$$\tilde{\alpha} = \begin{cases} 0 & \text{for} \quad \eta_c \leq \eta \leq 0 \\ 1/3 & \text{for} \quad \eta > 0 \end{cases} \tag{8}$$

and

$$\tilde{\beta} = \begin{cases} 1 & \text{for} \quad \eta_c \leq \eta \leq 0 \\ 1 - \frac{1}{\eta_t}\eta & \text{for} \quad 0 < \eta < \eta_t \\ 0 & \text{for} \quad \eta \geq \eta_t \end{cases} \tag{9}$$

while a simple linear relation for $\tilde{\beta}$ between 0 and η_t is used [12, 14, 15]. It is important to notice that it is not possible to study all influences experimentally, especially the Lode parameter dependence [6] is difficult to be detected and thus further micro-mechanical studies are necessary. The damage softening behavior is characterized by

$$\sigma\left(\mu, \dot{\mu}, \theta\right) = \tilde{\sigma}\left(\mu\right) f_3\left(\dot{\mu}\right) f_2\left(\theta\right) \tag{10}$$

using the multiplicative decomposition in analogy to the decomposition used for plastic hardening in Eq. (2) into a quasi-static $\tilde{\sigma}\left(\mu\right)$, a strain-rate-dependent $f_3\left(\dot{\mu}\right)$ and a temperature-dependent part $f_2\left(\theta\right)$. Here it can be noticed, that these relations lead to acceptable numerical results which could not be experimentally verified and hence need

to be studied in detail by numerical simulations on the micro-scale. In detail the rate-independent softening function is chosen to be quadratic in μ to

$$\tilde{\sigma}\left(\mu\right) = \frac{-\left(\tilde{H}_o \mu_e + \tilde{\sigma}_o\right)}{\mu_e^2} \mu^2 + \tilde{H}_o \mu + \tilde{\sigma}_o \tag{11}$$

and diagramed in Fig. 3 where $\tilde{\sigma}_o$ represents the initial damage strength, μ_e the fictitious value where the damage softening relation reaches zero and $\tilde{H}_o$ represents the slope of the static plastic hardening function (Eq. (3)) taken at the onset of damage [16]. Furthermore,

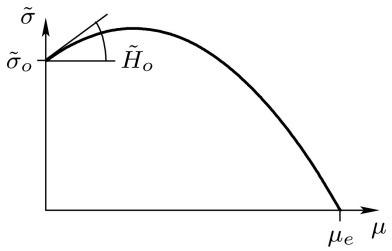

Figure 3: Damage softening law

the damage strain rate behavior is characterized by

$$f_3\left(\dot{\mu}\right) = 1 + h\left(\frac{\dot{\mu} - \dot{\mu}_o}{\dot{\mu}_o}\right)^r \tag{12}$$

where $\dot{\mu}_o$ is the reference damage strain rate and h as well as r are further material parameters.

Moreover, the internal damage variable μ can be used to define a simple triaxiality-dependent fracture criterion [14]. The corresponding fracture condition can be written in the form

$$f^{\mathrm{cr}} = \mu - \mu_{\mathrm{cr}} = 0 \tag{13}$$

where μ_{cr} is the triaxiality-dependent critical equivalent damage strain:

$$\mu_{\mathrm{cr}} = \begin{cases} \mu_f & \text{for} \quad \eta > \eta_f \\ \frac{\mu_f - \mu_o}{\eta_f}\eta + \mu_o & \text{for} \quad 0 \leq \eta \leq \eta_f \\ \mu_o & \text{for} \quad \eta < 0. \end{cases} \tag{14}$$

The introduced material parameters μ_f and μ_o represent the critical tension and compression values of the equivalent damage strain while η_f is the fracture transmission triaxiality. With this, relatively simple, fracture criterion it is possible to simulate the complete failure process until final fracture. But it is important to keep in mind, that this criterion

is not experimentally verified and that new micro-mechanical studies may lead to new insights into this process and thus to a modification of the fracture criterion.

The presented material model has been successfully used to simulate material behavior under dynamic loading conditions [12, 16]. Within these studies remarkable differences within the damage evolution considering the strain-rate-dependence or not have been detected. Furthermore, the determination as well as its physical interpretation of the corresponding damage parameters was found to be difficult with the available experimental data while static micro-mechanical simulations were found to be useful for the determination of damage condition and damage rule [6]. Thus, in continuation, micro-mechanical simulation of pore containing cells under dynamic loading conditions are presented.

3 DYNAMIC MICRO-MECHANICAL SIMULATIONS

The micro-mechanical numerical studies are applied to predict the damage and fracture process under dynamic loading conditions as they are shown, for instance, in Fig. 1. This process of material deterioration of ductile metals is characterized through void growth, nucleation and coalescence at stress states with higher hydrostatic-pressures and through the occurrence of micro-shear-bands [2, 13] which result in a macro-crack and hence in the failure of the material. These studies are realized withe LsDyna considering elastic-plastic material with linear hardening (MAT_12) while the material parameters correspond to an aluminum alloy used in aircraft production.

These (first) micro-mechanical studies under dynamic loading conditions focus on void growth of uniaxially loaded micro-cells. The numerical model consists of three sections, Fig. 4a, having a length of $60\,\mu$m in each direction which reflects realistic physical dimensions. Following the ideas of Benson [7], only the central part of the model, where the damage processes are studied, contains micro-pores, Fig. 4b, while the initial and the final region are homogeneous, allowing an undisturbed wave propagation. Moreover the model is loaded by a trapezoidal tension pulse in x-direction which is similar to the pulse occurring in a Split-Hopkinson-Bar experiment [17]. This pulse has a total duration of $0.07\,\mu$s while the maximum loading lasts for $0.05\,\mu$s.

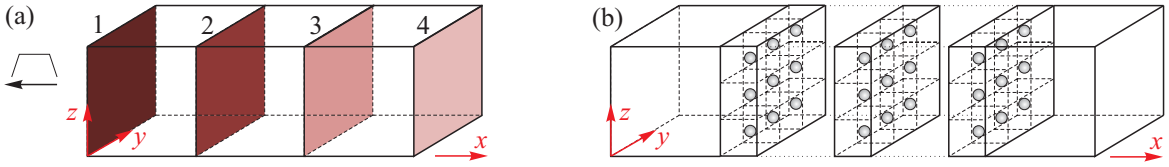

Figure 4: Numerical model with micro-pores

Previous to the studies with pre-damaged material, the influence of different boundary conditions is studied. Here it is important to keep in mind, that the studied model is supposed to be a cut-out from a major material sample. For this study homogeneous, i.e. undamaged, material is loaded with a 1 N pulse at which the material respond is

purely elastic. Figure 5 displays the applied boundary conditions as well as the summed forces in x-direction in different cuts as indicated in Fig. 4a and the summed forces of the central part in the directions perpendicular to the loading direction. The sketch illustrating the boundary conditions uses the following symbolism: a dashed line represents the undeformed model, a heavy solid line indicates the deformed shape, a thin dotted line represents coupled degrees of freedom perpendicular to the line while a heavy thick line indicates zero displacements and finally tildes indicate that flow out boundary conditions are applied.

The boundary conditions applied in Fig. 5a and Fig. 5b clearly indicate a non uniform displacement field perpendicular to the loading direction and thus the sample can not be seen as a cut-out of a bigger sample. The flow-out boundary conditions perpendicular to the loading direction indicated in Fig. 5b lead to remarkable reduction of the pulse intensity throughout the specimen in length direction which also disagrees with existing conditions within a bigger sample. The boundary conditions indicated in Fig. 5c do not permit any reduction of the cross section perpendicular to the loading condition which results into remarkable forces in these directions and consequently the resulting stress state is not uniaxial. This effect becomes even more significant for higher loads while material reaction is elastic-plastic due to plastic incompressibility, Fig. 6. The boundary conditions indicated in Fig. 5d allow a reduction of the cross section where boundary nodes perpendicular to the loading direction are coupled in the corresponding direction which can be seen in contrast to the idea of a cut-out from a bigger sample. Overall the choice of the appropriate boundary conditions is more complex as in the static case [6] and although only loading in one direction is considered, the choice is always a compromise in some sense. In continuation all studies have been realized with the boundary conditions indicated in Fig. 5c which appeared to be the most appropriate one.

The simulations with pre-damaged material are realized with a constant initial porosity of 3% in relation to the volume of the central part. For this purpose the central part is overlaid with a 3 by 3 by 3 raster (Fig. 4b) where each cell can contain one spherical void at its center while all voids are assumed to have the same radius. Hence, if not all cells contain pores, the pore radius increases. This approach allows to study the behavior of homogeneously distributed pores and first influences of the pore distribution while completely randomly distributed pores and different pore diameters are not considered here. Corresponding meshes are displayed in Fig. 7.

Simulations with homogeneous pore distributions as displayed in Fig. 4b indicate that the pores within the first layer enlarge remarkably before the wave propagates further. Figure 8 shows this behavior clearly at time $0.034\,\mu$s. It is important to notice that the undamaged initial part only deforms elastically while the maximum plastic deformations of the pre-damaged part already reaches about 12%. Obviously within this pore layer already pore coalescence, which is not considered here, would take place and a study with a reduces number of pores, which can be distributed in several ways, is evident.

For this study a total of 5 pores has been chosen which are collocated in several dif-

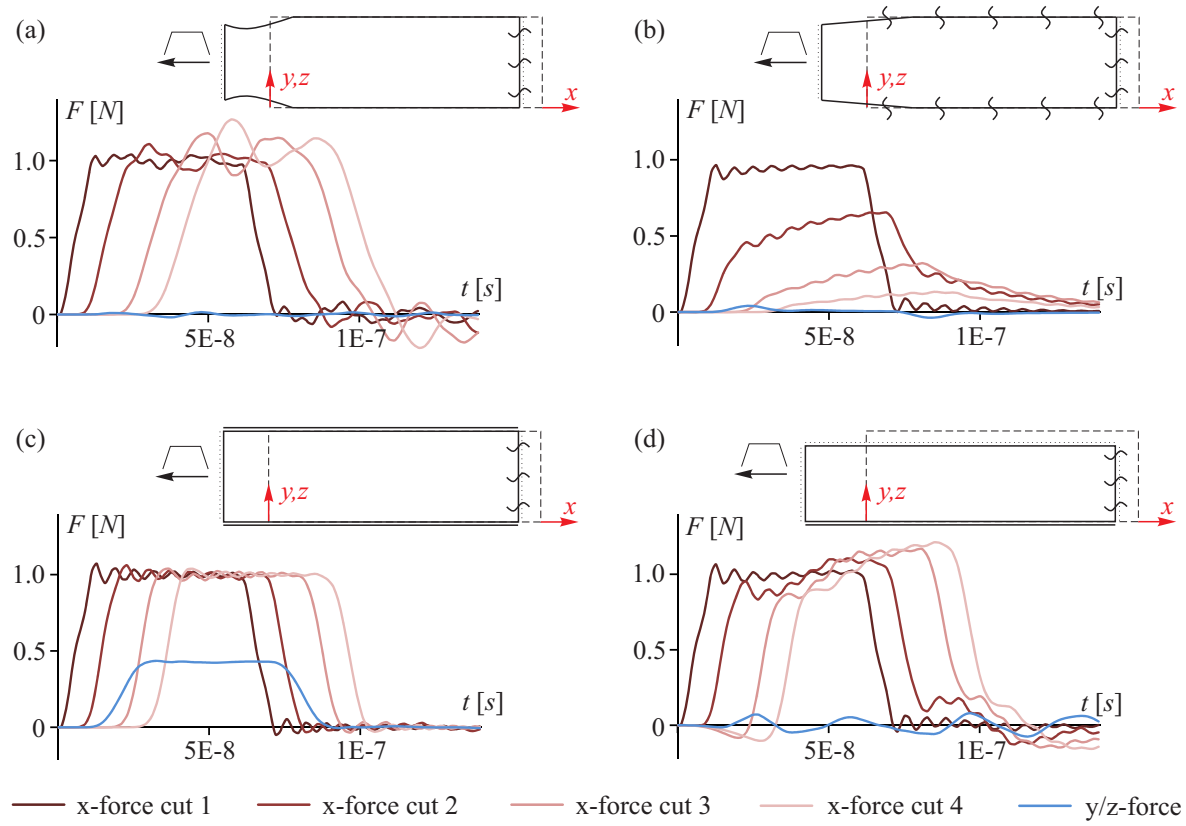

Figure 5: Resulting forces at different boundary conditions

ferent ways; amongst others Fig. 9 displays three choices. The crosswise distribution perpendicular to the loading direction (Fig. 9a) as well as in loading direction (Fig. 9c) may facilitate shear mechanisms as indicated for instance in Fig. 10. This shear stress concentration is an indicator for pore interaction which can lead finally to coalescence. Furthermore the distribution indicated in Fig. 9b leads to a concentration of plastic deformations where no pore is collocated in the second layer (Fig. 11), i.e. a micro crack is induced here, while the pores in the second layer reduce the plastic strain concentration. It is important to notice that different pore distributions may lead to different fracture mechanisms and that a critical distribution was not identified. In addition, the definition of a micro-crack criterion, i.e. where the pore interaction progresses are included, may even change the results significantly.

4 CONCLUSIONS

With the presented numerical analysis it was possible to study the damage process under dynamic loading conditions in detail. Big effort was made to find the most appropriate boundary conditions to study the material behavior at the center of an extensive sample with a reduced model. Furthermore it was found that the pore distribution has

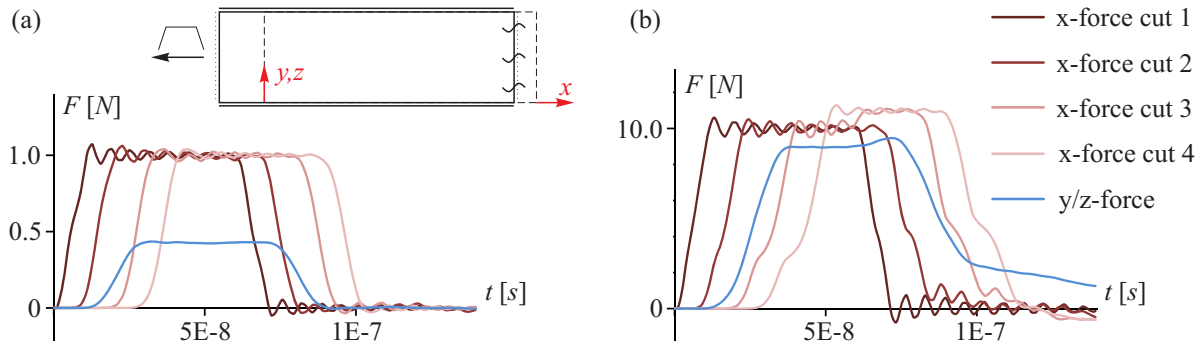

Figure 6: Resulting forces of an elastic (a) and an elastic-plastic simulation (b)

a significant influence on the resulting deformation and thus on the stress state of the material which will lead to significantly different micro-failure processes. Hence, further studies to identify critical pore distributions and to identify the corresponding failure processes are necessary.

Overall it can be stated that a straight forward approach from static loading [6] to dynamic loading is not possible. Especially the definition of the appropriate boundary conditions, the controlled generation of stress states, which will become even more critical for three-dimensional loading and the definition of a micro-fracture criterion will need special attention.

REFERENCES

[1] T. W. Barbee, L. Seaman, R. Crewdson, and D. Curran. Dynamic fracture criteria for ductile and brittle metals. *Journal of Materials*, 7:393–401, 1972.

[2] M. Brünig, O. Chyra, D. Albrecht, L. Driemeier, and M. Alves. A ductile damage criterion at various stress triaxialities. *International Journal of Plasticity*, 24:1731–1755, 2008.

[3] X. Gao, T. Zhang, M. Hayden, and C. Roe. Effects of the stress state on plasticity and ductile failure of an aluminum 5083 alloy. *International Journal of Plasticity*, 25:2366–2382, 2009.

[4] A. Needleman. Void growth in an elastic-plastic medium. *Journal of Applied Mechanics*, 4:964–970, 1972.

[5] M. Kuna and D.Z. Sun. Three-dimensional cell model analyses of void growth in ductile materials. *International Journal of Fracture*, 81:235–258, 1996.

[6] M. Brünig, S. Gerke, and V. Hagenbrock. Micro-mechanical studies on the effect of the stress triaxiality and the Lode parameter on ductile damage. *International Journal of Plasticity*, 50:49–65, 2013.

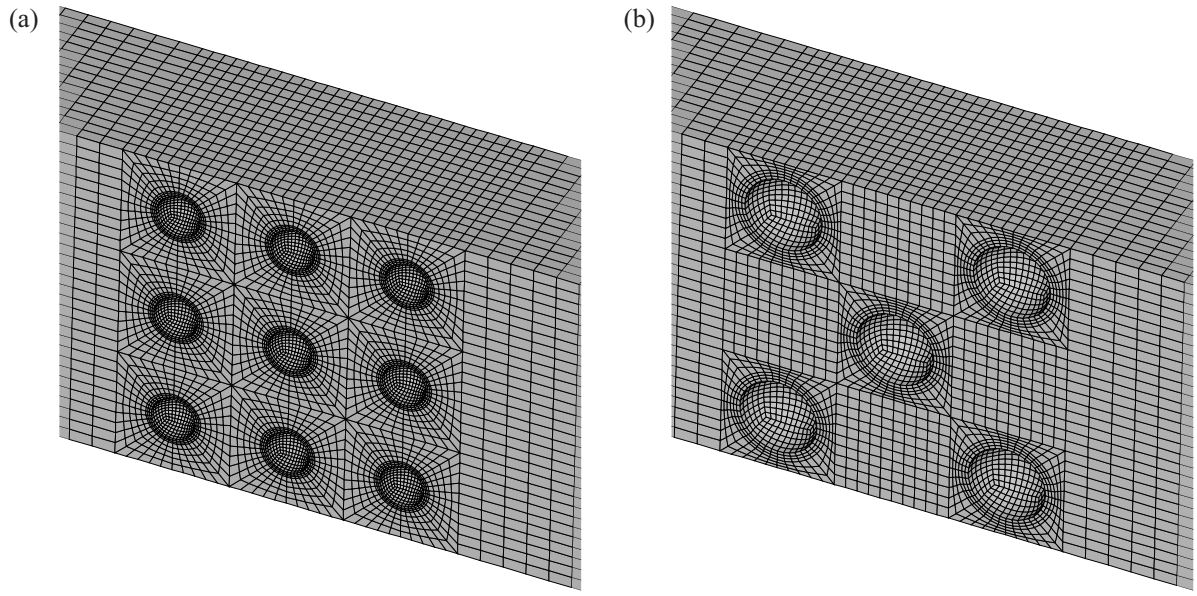

Figure 7: Mesh: (a) of a homogeneous pore distribution with 27 pores and (b) of a heterogeneous pore distribution as indicated in Fig. 9b with 5 pores

[7] D. J. Benson. An analysis of void distribution effects on the dynamic growth and coalescense of voids in ductile metals. *Journal of the Mechanics and Physics of Solids*, 41:1285–1308, 1993.

[8] M. Brünig. An anisotropic ductile damage model based on irreversible thermodynamics. *International Journal of Plasticity*, 19:1679–1713, 2003.

[9] M. Brünig. Continuum framework for rate-dependent behavior of anisotropic damaged ductile metals. *Acta Mechanica*, 186:37–53, 2006.

[10] W. A. Spitzig, R. J. Sober, and O. Richmond. The effect of hydrostatic pressure on the deformation behavior of maraging and HY-80 steels and its implications for plasticity theory. *Metallurgical Transactions A*, 7A:1703–1710, 1976.

[11] G. R. Johnson and W. H. Cook. A constitutive model and data for metals subjected to large strains, high strain rates and high temperatures. In *Proceedings of the Seventh International Symposium on Ballistics, Hague, Netherlands*. American Defense Preparedness Association; Koninklijk Instituut van Ingenieurs (Netherlands), 541–547, 1983.

[12] S. Gerke. *Damage and fracture of ductile metals under dynamic loading conditions*. PhD thesis, Universität der Bundeswehr, München, 2013.

[13] Y. Bao and T. Wierzbicki. On the fracture locus in the equivalent strain and stress triaxiality space. *International Journal of Mechanical Sciences*, 46:81–98, 2004.

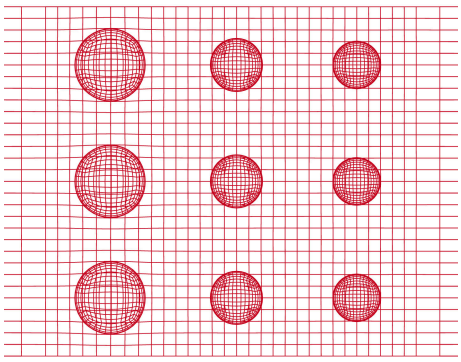

Figure 8: Pore growth of homogeneous distribution

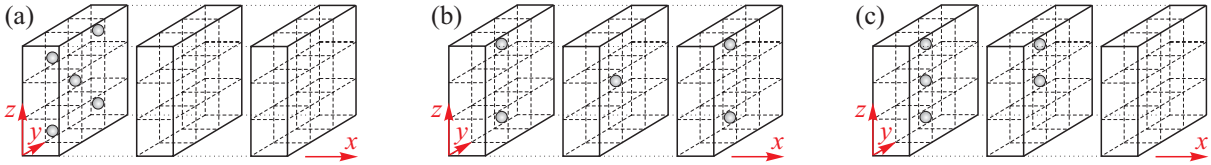

Figure 9: Pore distribution

[14] M. Brünig, D. Albrecht, and S. Gerke. Modelling of ductile damage and fracture behavior based on different micromechanisms. *International Journal of Damage Mechanics*, 20:558–577, 2011.

[15] M. Brünig, D. Albrecht, and S. Gerke. Numerical analyses of stress-triaxiality-dependent inelastic deformation behavior of aluminium alloys. *International Journal of Damage Mechanics*, 20:299–317, 2011.

[16] M. Brünig and S. Gerke. Simulation of damage evolution in ductile metals undergoing dynamic loading conditions. *International Journal of Plasticity*, 27:1598–1617, 2011.

[17] W. W. Chen and B. Song. *Split Hopkinson (Kolsky) bar; design, testing and applications*. Spinger, 2011.

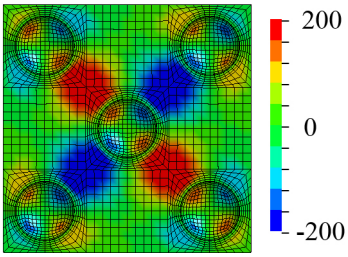

Figure 10: Shear stresses of pore distribution as displayed in Fig. 9a; cut in y/z-plane

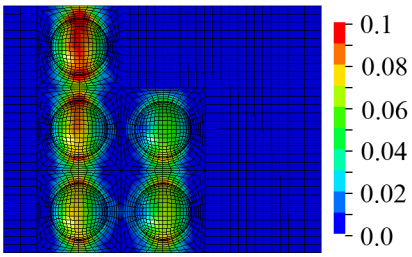

Figure 11: Plastic strains of pore distribution as displayed in Fig. 9c; cut in x/z-plane